ACS APPLIED MATERIALS & INTERFACES

Research Article

www.acsami.org

Hybrid Transparent Conductive Film on Flexible Glass Formed by Hot-Pressing Graphene on a Silver Nanowire Mesh

Tong Lai Chen,*[,†] Dhriti Sundar Ghosh,[†] Vahagn Mkhitaryan,[†] and Valerio Pruneri[†,‡]

[†]ICFO−Institut de Ciencies Fotoniques, Mediterranean Technology Park, Castelldefels, Barcelona 08860, Spain

[‡]ICREA- Institució Catalana de Recerca i Estudis Avançats, Barcelona, 08010, Spain

Supporting Information

ABSTRACT: Polycrystalline graphene and metallic nanowires (NWs) have been proposed to replace indium tin oxide (ITO), the most widely used transparent electrode (TE) film on the market. However, the trade-off between optical transparency (T_{opt}) and electrical sheet resistance (R_s) of these materials taken alone makes them difficult to compete with ITO. In this paper, we show that, by hot-press transfer of graphene monolayer on Ag NWs, the resulting combined structure benefits from the synergy of the two materials, giving a T_{opt}−R_s trade-off better than that expected by simply adding the single material contributions Ag NWs bridge any interruption in transferred graphene, while graphene lowers the contact resistance among neighboring NWs and provides local conductivity in the uncovered regions in-between NWs. The hot-pressing not only allows graphene transfer but also compacts the NWs joints, thus reducing contact resistance. The dependence on the initial NW concentration of the effects produced by the hot press process on its own and the graphene transfer using hot press was investigated and indicates that a low concentration is more suitable for the proposed geometry. A TE film with T_{opt} of 90% and R_s of 14 Ω/sq is demonstrated, also on a flexible glass substrate about 140 μm thick, a very attractive platform for efficient flexible electronic and photonic devices.

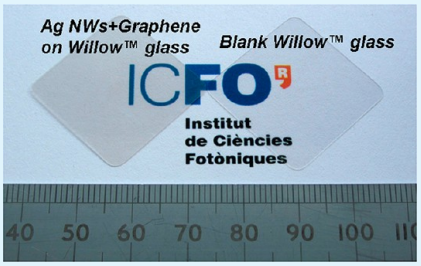

KEYWORDS: *nanowires, transparent electrodes, ITO-free, graphene, hot-pressing*

INTRODUCTION

Transparent electrodes (TEs) are one of the essential elements for a wide range of optoelectronic devices and components, such as rigid displays, touch panels, light emitting diodes, and solar cells. Indium tin oxide (ITO) is the most widely used TE since it possesses high optical transparency (T_{opt}, referred herein as the transmittance with substrate contribution subtracted) and low sheet electrical resistance (R_s). However it presents several drawbacks, including fluctuating high cost due to indium scarcity, chemical instability associated with indium migration when combined with certain materials, and lack of mechanical flexibility due to its fragility.[1−6]

The development of one or two-dimensional (1D or 2D) nanostructured materials, such as Cu or Ag nanowires (Cu or Ag NWs), carbon nanotubes, and graphene, has allowed the realization of ITO-free TEs.[7−17] More recently roll-to-roll (R2R) and hot-pressing production of grapheme based TEs has been demonstrated, offering a good trade-off between T_{opt} and R_s.[18,19] Both R2R and large-area hot-pressing are potentially efficient and economical, thus suitable for industrial-scale applications requiring low cost and high throughput production. The most recent laboratory data on electrical conductivity of monolayer graphene is still far from the performance of conventional ITO or doped ZnO layers, which typically have R_s values in the 10−30 Ω/sq range.[20−22] In transferred graphene, intrinsic line defects and disruptions, such as wrinkles, ripples, or foldings, as well as grain boundaries, generated radicals, and residual O-containing groups, can significantly influence the transport properties, causing a large deviation from the theoretical value for a given level of doping. In fact, Jeong et al.[23] have proposed that an alleviation of the detrimental effects of these defects can be obtained through the integration of 1D metal NWs with graphene. Kholmanov et al.[24] also recently reported a hybrid TE based on graphene/Ag NWs, where the electrical conductivity of graphene was enhanced by the presence of Ag NWs.

Recently, also TEs based on randomly perforated Ag NWs mesh have attracted considerable attention due to their easy large-area fabrication (e.g. spray coating), high electrical conductivity, and mechanical flexibility. However, effective connections between Ag NWs should be well addressed prior to their applications, this being a critical parameter to achieve low R_s. Several methods have been proposed to improve the contacts between Ag NWs, including thermal annealing,[9,10] mechanical pressure,[25−27] and vacuum filtration.[28] Another issue is related to the voids in between Ag NWs, which can lead to parasitic current flow/crowding and problems of charge extraction/injection of the electrode.[29] It is thus desirable filling the voids with electrically conductive material for improving the performance of devices using Ag NW TEs. In addition, the density of Ag NWs must heavily exceed the percolation threshold to achieve suitably low values of R_s. This leads to a

Received: August 16, 2013
Accepted: October 28, 2013
Published: October 28, 2013

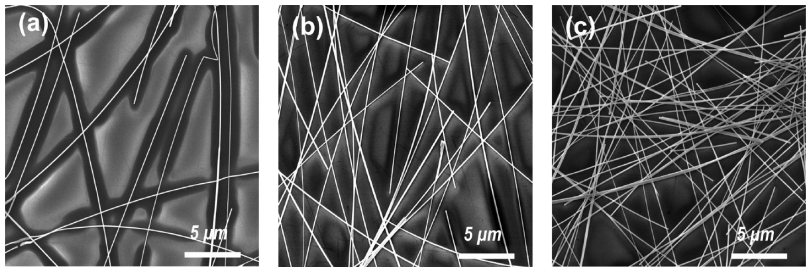

Figure 1. Commercially available Ag NWs (dispersed in IPA with different NWs concentrations) were spin-coated onto flexible glass substrates (Corning Willow glass). The films were then dried naturally in a fume-hood at room temperature. (a) A1, (b) A2, and (c) A3.

reduction in T_{opt} and also increases the scattering (haze), this latter aspect being related to the random nature and size of the Ag NWs. An increase in the haze reduces the clarity of the TE and for some applications this is a detrimental effect, for example in touch-screens and displays.[30] In this paper, we report a hybrid TEs on flexible glass substrate consisting of hot-pressing transferred monolayer graphene onto Ag NWs mesh. We experimentally demonstrate that the combination of hot-pressing transferred monolayer graphene and Ag NWs mutually benefit these two nanomaterials. On the one hand, Ag NWs can minimize the influence of defects and disruptions presented in transferred graphene by forming a continuous conducting network while, on the other hand, graphene offers a conformal coverage and full encapsulation of Ag NWs mesh to improve local conductivity in between the NWs as well as reduce their contact resistance. Contrary to previous reports[23,24] in which the graphene was transferred via wet-transfer, the hot-pressing method employed in this work presents several advantages, including large-area fabrication, contact resistance reduction by increasing the strength of the NW junctions and better adhesion to the substrate thanks to the application of a conformal mechanical pressure. The result is a Ag NWs/graphene based TE with R_s of about 14 Ω/sq and T_{opt} of about 90%, which is an electro-optical performance comparable to commercially available ITO.

EXPERIMENTAL DETAILS

Sample Preparation. A flexible glass substrate (Corning® Willow glass, 140 μm thick, available from Corning Incorporated, Corning, NY) is used instead of normal rigid glass or polymer substrates. With respect to conventional flexible polymer substrates (such as polyethylene terephthalate (PET), polyethylene naphthalate (PEN)), Willow glass provides the higher performance of any glass, can sustain higher-processing temperatures, and has superior antipermeation properties against oxygen and moisture and similar mechanical flexibility, making it compatible with R2R manufacturing processes. Ag NWs were commercially purchased from Seashell Tech. (California) with concentrations of 25 mg/mL in isopropanol (IPA) and average diameter of 100 nm and length of 20−40 μm. The Ag NW dispersed solution was diluted down to the required concentration by adding IPA. Ultrasonic bath of the NW solution should be avoided as it leads to the breaking of the NWs. Corning Willow glass substrates (140 μm thick, 1 inch square) were cleaned in acetone followed ethanol in ultrasonic bath, each process lasting 10 minutes. The substrates were then rinsed in abundant DI water and dried with nitrogen gas followed by oxygen plasma for 150 seconds. The NW films were then prepared by single step spin-coating (2000 rpm) of the dispersed NW solution. By varying the concentration of the NWs in the solution, the electro-optical properties of the film could be tuned. Typical SEM images for the films with different NWs concentration (denoted with A1, A2, and A3) are shown as Figure 1. The NWs concentrations for these three diluted solutions are about 2.5, 4.0, and 5.4 mg/mL for A1, A2, and A3, respectively.

Graphene Transfer. Monolayer graphene on Cu foils were purchased from Graphenea. Thermal release tape (TRT) was placed on the graphene/Cu foil, and then, the Cu foil was etched at room temperature by an aqueous iron(III) chloride ($FeCl_3$) solution (1 M). The graphene on TRT was attached to the target substrates of Ag NWs coated glass substrates. The TRT/graphene film/target substrate was put between the two metal plates in the hot-pressing set-up to apply the pressure and heating (up to 130 °C). In the hot press process, a pressure of about 500 psi is applied for 30 seconds. After the transfer process, the TRT lost adhesion force and then can be easily peeled off, resulting in the graphene film transferred onto the target substrate. The transferred monolayer graphene on plain glass substrate shows a R_s of 1.3±0.2 kΩ/sq. This value is comparable to data reported in the literature that they use a PMMA-assisted wet-transfer method.[31]

Characterization. The electrical properties of the films were measured using four-point probe method with cascade Microtech 44/7 S 2749 probe system attached to a Keithley 2001 multimeter. Typically, six measurements were performed at different positions on the films and mean value were used to calculate the R_s. A Perkin Elmer lambda 950 spectrometer was used for optical transmission measurements. The Haze factor was measured using a WGT-S luminous transmittance/haze test instrument. The surface morphology of the films was done with the help of FEI-SEM and Vecco AFM. The optical transparency herein refers as the transmittance with substrate contribution subtracted [transmittance of (graphene/Ag NWs/substrate)/transmittance of substrate]. The quality of the transferred graphene films was assessed using Raman spectroscopy (Renishaw InVia Raman microscope, 532 nm laser and 100× objective lens).

RESULTS AND DISCUSSION

The combination of graphene with Ag NWs is schematically shown in Figure 2a and b. Figure 2c demonstrates the flexibility of a piece of Willow glass with the proposed TE, and Figure 2d shows two samples images: one is a blank Willow glass (right) and the other one with the hybrid graphene/Ag NWs on Willow glass (left). As it was mentioned above, the as-deposited Ag NWs require extra treatments, including thermal annealing and/or mechanical pressing, to enhance the connection between the NW junctions and improve their electrical

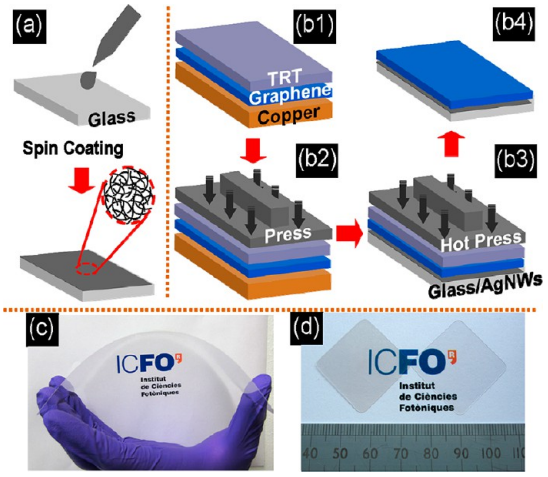

Figure 2. Fabrication of graphene/Ag NWs on flexible substrates. (a) Spin-coating of Ag NWs solution onto flexible glass. (b) Hot-pressing transfer process for the hybrid film: thermal release tape (TRT) was placed on the graphene/Cu foil (b1), and then the Cu foil was etched at room temperature by an aqueous iron(III) chloride ($FeCl_3$) solution (1 M) (b2). The graphene on TRT was attached to Ag NWs coated glass substrates (b3). After the transfer process, the TRT loses adhesion force at elevated temperature and then can be easily peeled off, resulting in the graphene film transferred onto the target substrate (b4). (c) Photograph of a piece of flexible Willow glass substrate with proposed TE. (d) Photograph of a 1 in. ×1 in. blank Willow glass (right), and the hybrid graphene/Ag NWs on Willow glass substrate (left).

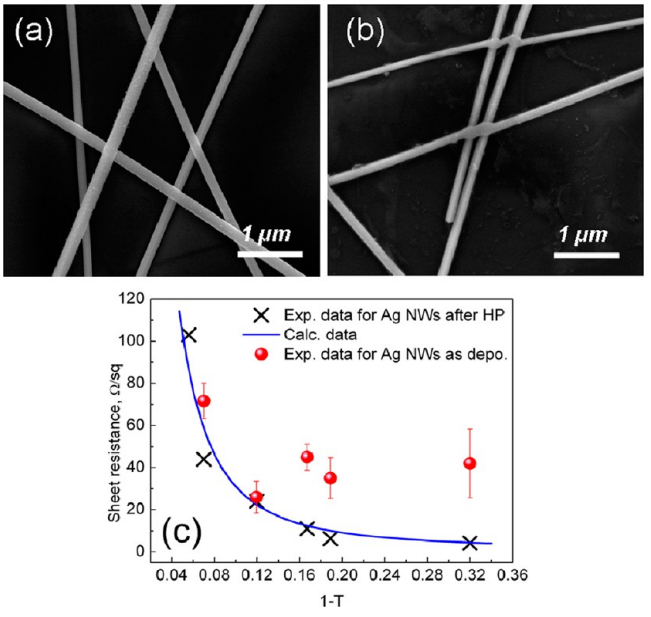

Figure 3. Effect of hot-pressing on the NWs junctions. (a) For as-deposited Ag NWs junctions, the NWs were randomly dispersed and loosely connected to each other. After the hot-pressing treatment, NWs junctions can be compacted to form an intimate contact with each other in some areas as well as flattened by the pressure (b). The calculated data (denoted as the blue curve), along with two sets of experimental data on Ag NWs (c). One set of the data represents the transparency (at the wavelength of 550 nm) and sheet resistance (R_s) values for Ag NWs as deposited without any treatment, and the other set of data correspond to Ag NWs after the hot-pressing treatment without graphene transfer.

conductivity. Therefore, it is very beneficial that the hot-pressing transfer process of graphene onto Ag NWs provide pressure and heating at the same time. Figure 3 shows the effect of hot-pressing on the NWs junctions. For as-deposited Ag NWs junctions, the NWs were randomly dispersed and loosely connected to each other (Figure 3a). In contrast, after the hot-pressing treatment, NWs junctions can be compacted to form an intimate contact with each other and in some parts the applied pressure can even flatten the junction between Ag NWs, thus increasing the contact area (Figure 3b). This effect is followed by a significant reduction in R_s of sample A2. After only hot-pressing, before applying graphene, R_s goes from 71.7 to 44 Ω/sq.

We also studied and calculated the co-relation between R_s and T_{opt} of Ag NW mesh to better design the TE geometry. There have been two main theoretical models to describe the conductivity of such 1D nanowire mesh. One is based on the percolation theory,[32] in which the effective electrical conductivity σ_e can be calculated using the following formula:

$$\frac{\sigma_e}{\sigma_m} = 1 + \frac{f}{3}\left(\frac{1}{(\sigma_3/\sigma_m - 1)^{-1} + H} + \frac{2}{(\sigma_1/\sigma_m - 1)^{-1} + (1 - H)/2}\right) \quad (1)$$

where σ_3 and σ_1 denote the axial and transverse electrical conductivities of the 1D nanostructure mesh, f represents the effect from the isotropic matrix in which the nanowires are embedded, and H reflects the influence of the aspect ratio $p = L/d$ (L and d are the length and diameter of NWs, respectively). Detailed information about this model can be found in refs 32 and 33. The second model describes the electron transport in any 1D nanowire mesh as a random walk.[34] The electrical conductivity can be expressed as follows:

$$\sigma = \sigma_0 h\left[1 - \frac{b}{2h\sqrt{\ln \alpha}} \tanh\left(\frac{2h\sqrt{\ln \alpha}}{b}\right)\right] \quad (2)$$

where $\sigma_0 h$ is the bare conductivity of an average conductive path, and h and b denote the vertical distance between random walk steps and step length, respectively. α is the relative factor associated with a finite reduction in conductivity.

We have carried out calculations by combining these two theories to have a full description of 2D nanowire mesh. In eq 2, we replaced σ_0 with σ_e expressed in eq 1, and this substitution can predict not only percolation properties, but also the dependence of R_s upon the thickness, which subsequently correlates optical transmittance through the Beer–Lambert Law.

Figure 3c shows the calculated data (blue curve), along with two set of experimental data. One set of the data represents T_{opt} (at the wavelength of 550 nm) and R_s values for Ag NWs as deposited without any treatment while the other set the corresponding values for Ag NWs after the hot-pressing treatment, without graphene transfer. As deposited Ag NWs meshes are randomly dispersed and loosely connected, and as a result, the measured R_s were not very stable, as it is shown by relatively large error bars in the measurements. On the contrary, after the hot-pressing treatment, the measurements for R_s showed very good stability and repeatability, and the data are in excellent agreement with theoretical predictions, suggesting that hot-pressing process can serve as an effective way to obtain stable and robust Ag NW based TEs.

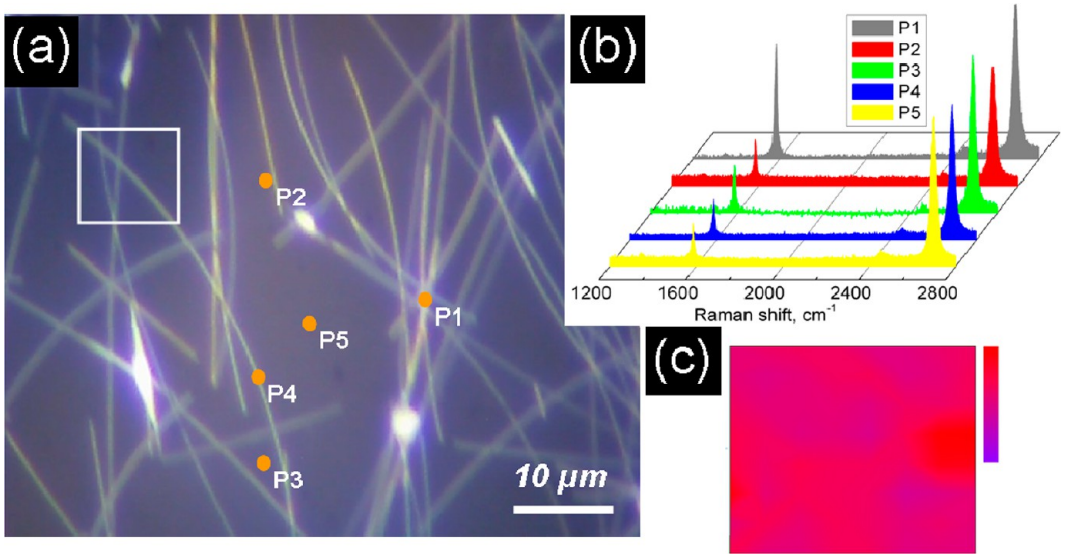

Figure 4. (a) Typical optical microscopy image of sample A2 in several points and a solid square corresponding to the Raman spectra for single-run operations and mapping image in parts b and c, respectively. Five positions (spots) were chosen for single-run with Raman spectroscopy, and the corresponding profiles are presented in part b. G and 2D peaks can be clearly observed in all the spectra, with negligible defect-related peaks, such as D and Ḋ. (c) Raman mapping, corresponding to the marked square area in part a, around the 2D mode of the transferred graphene. The selected areas show detectable intensities of the Raman signal (the areas between two neighboring Ag NWs, across single Ag NW, and at the top of the junction, respectively), indicating full coverage and encapsulation of Ag NWs mesh by graphene.

Various transfer methods for CVD-grown graphene have been recently developed, including micromechanical exfoliation,[35] poly-(methyl-methacrylate) (PMMA),[36] or polydimethylsiloxane (PDMS) assisted processing,[37] R2R,[18,38] and hot-pressing.[19] As it was mentioned above, graphene hot-pressing transfer method can provide additional pressure and temperature to the underlying Ag NWs. Figure 4a shows a typical optical microscopy image of sample A2 in several marked positions, corresponding to which Raman spectra were taken. Five positions (spots) were chosen for single-run operation Raman spectroscopy (Figure 4a), and the corresponding image profiles are presented in Figure 4b. G and 2D peaks can be clearly observed in all spectra, with negligible defect-related peaks, such as D and Ḋ. The G/2D peak-intensity ratios for the five spots (P1 to P5) are 0.746, 0.39, 0.303, 0.299, and 0.288, respectively. In P1 (multi-junction of Ag NWs) the transferred graphene shows a higher G/2D ratio, suggesting occurrence of graphene folding and wrinkles.[39] In the others positions, the G/2D ratio varies in a very small range from 0.288 to 0.39, suggesting a very good quality of the transferred graphene.[40] Figure 4c is the Raman mapping, corresponding to the marked square area in Figure 4a, around the 2D mode of the transferred graphene. The selected areas show detectable intensities of the Raman signal (the areas between two neighboring Ag NWs, across single Ag NW, and at the top of the junction, respectively), indicating full coverage and encapsulation of Ag NWs mesh by graphene. From these results, it can be concluded that the hot-press transferred continuous monolayer graphene fully covers the low-density concentration area of Ag NWs, while at areas of higher concentrated NW clusters, some graphene imperfections (such as foldings, cracks, wrinkles, etc.) are present. It should be noted that, for this work, Ag NWs with average diameter of 100 nm were used and imperfections of transferred graphene can be minimized with the use of smaller diameters. Two typical SEM images of the hybrid films (graphene capped Ag NWs mesh) are shown in Figure 5. Figure 5a shows the typical cluster of Ag NWs, while Figure 5b shows sparsely distributed Ag NWs mesh. As predicted from Raman spectra, graphene foldings/wrinkles is observed in Figure 5a, while in Figure 5b, it can be observed that the graphene layer follows the curvature of the underlying Ag NWs, providing an intimate contact in the hybrid film, which definitely improves local charge injection and collection between adjacent NWs.

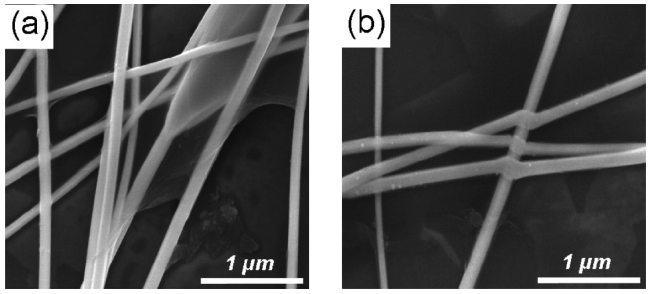

Figure 5. Two typical SEM images of the hybrid films (graphene capped Ag NWs). (a) shows the typical cluster of Ag NWs, while (b) shows sparsely distributed Ag NWs mesh. As predicted from Raman spectra, graphene foldings/wrinkles is observed in part a, while in part b it can be appreciated that the graphene layer follows the curvature of the underlying Ag NWs, providing an intimate contact in the hybrid film, which significantly improves local charge injection and collection between adjacent NWs.

The optical transparency of the graphene/NW hybrid films was investigated. Sample A2 shows an average T_{opt} higher than 90%, and after capping with a monolayer graphene, the value is reduced by around 2.3%, which corresponds to the intrinsic optical absorption of single-layer graphene, equivalent to $\pi\alpha$, where α is the fine structure constant. With an increase in NWs concentration, sample A3 shows a much lower transparency compared to sample A2 (about 5%), as well as an increase in average scattering, haze increased from around 3.8% to 4.6%. The haze presented in this study can be beneficial in photovoltaic cells, because if properly tailored it could lead to

enhanced interaction and absorption with the active layer inside the cell. The haze can be easily tailored by modifying the NW diameter and concentration, as it is evident by comparing samples A2 and A3 for example. The optical properties of the samples depend mostly on NW density, and the graphene capping only gives an optical transparency drop of about 2.3%. However, as it was previously shown, graphene capping changes radically the electrical properties of the samples.

Figure 6 summarizes the data for three different concentration Ag NWs samples, A1, A2, and A3, after only hot press

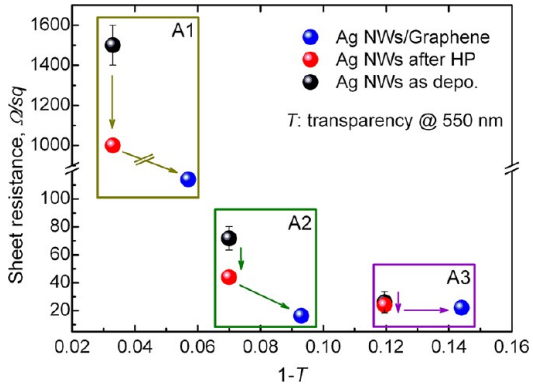

Figure 6. Summary of electro-optical performance for three typical Ag NW samples which have different concentrations of NWs. Reductions in sheet resistance for A1, A2, and A3 samples before and after graphene capping show very distinct trends. Resistance decrease ratio in A1 sample is very high(about 1300%), and a lower change in resistance (about 440%) is observed in sample A2. For sample A3, the changes are much smaller. It can be gathered that sparse Ag NWs mesh is more favorable for a good quality graphene transfer by hot-pressing and maximization of associated effects.

(no graphene transferred yet) and after graphene transfer using hot press. The resistance reduction due to graphene capping for samples A1 and A2 are very high, about 1300% and 440%, respectively. Instead, sample A3 shows a much larger reduction due to the hot pressing itself, with the additional reduction associated to the graphene capping very small. Therefore, it can be concluded that sparse Ag NWs meshes are more favorable for an effective graphene capping improvement during hot-press transfer. The resulting overall R_s for the hybrid A1 and A2 samples are 114 and 16.3 Ω/sq, respectively. In addition, the transparency at 550 nm is greater than 90 % in both cases. The obtained low R_s values for the hybrid films demonstrate that the Ag NWs bridge any interrupted electrical conductive path in transferred graphene thanks to their random dispersion and dimensions (length of tens of micrometers), comparable to the average CVD-grown graphene grain-size (about 10-20 μm).

The transparency (T_{opt} at the wavelength of 550 nm) and R_s of typical hybrid films of graphene/Ag NWs demonstrated so far (refs 24, 41, and 42), pure graphene (ref 43), and pure Ag NWs (ref 27) are summarized in Figure 7, together with our results (experimental and theoretical). As illustrated, the performance of our hybrid films of graphene/Ag NWs shows a competitive advantage in terms of trade-off between T_{opt} and R_s, in addition to the large-area fabrication possibility offered by the hot press processing.

CONCLUSIONS

We have investigated the combination of Ag NWs and graphene transferred by hot-pressing, showing that by

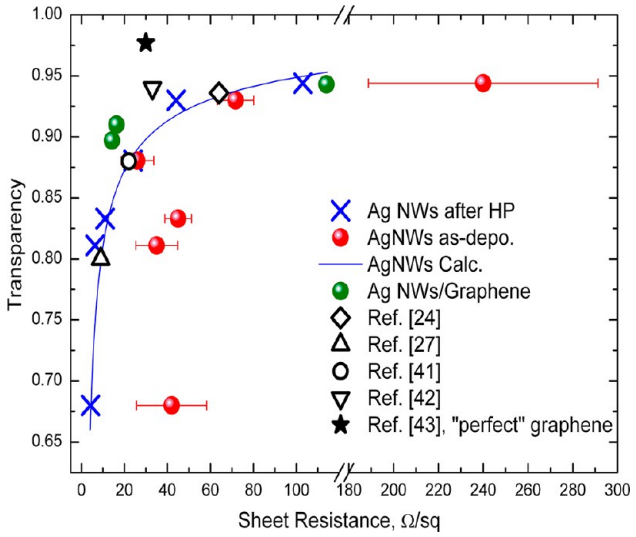

Figure 7. Transparency at 550 nm and sheet resistance of previously reported hybrid films of graphene/Ag NWs (refs 24, 41, and 42), pure graphene (ref 43), and pure Ag NWs (ref 27), together with our results (experimental and theoretical), showing the competitive advantage of the proposed geometry and method.

optimizing the initial concentration of the NWs in precursor solution and the hot-pressing conditions, high-performance transparent electrodes on flexible glass substrates can be realized. In particular, this approach is more convenient and effective when employing a low Ag NWs concentration (less than 5 mg/mL in precursor solution). Contrary to previous reports, the use of the hot-pressing allows improved results, large surface processing and at the same time, the flexible glass substrate, allows high performance, improved stability, and long lifetime for optoelectronic devices.

ASSOCIATED CONTENT

Supporting Information

Diameter and length distribution of the Ag NWs. This material is available free of charge via the Internet at http://pubs.acs.org.

AUTHOR INFORMATION

Corresponding Author

*E-mail: tonglai.chen@icfo.es.

Notes

The authors declare no competing financial interest.

ACKNOWLEDGMENTS

This work was supported by the Ministerio de Ciencia e Innovacion through Grant TEC2010-14832. T. L.C. also acknowledges the financial support from the Spanish Ministry of Education and Science through the Ramon y Cajal (RyC) fellowship. The authors thank Corning Incorporated for providing the Willow glass sheets.

REFERENCES

(1) Lecover, R.; Williams, N.; Markovic, N.; Reich, D. H.; Naiman, D. Q.; Katz, H. E. *ACS Nano* **2012**, *6*, 2865−2870.

(2) Ghosh, D. S.; Chen, T. L.; Pruneri, V. *Appl. Phys. Lett.* **2010**, *96*, 091106.

(3) Leever, B. J.; Murray, I. P.; Durstock, M. F.; Marks, T. J.; Hersam, M. C. *J. Phys. Chem. C* **2011**, *115*, 22688−22694.

(4) Ghosh, D. S.; Martínez, L.; Giurgulo, S.; Vergani, P.; Pruneri, V. *Opt. Lett.* **2009**, *34*, 325−327.

(5) Inganäs, O. *Nat. Photonics* **2011**, *5*, 201−202.
(6) Kumar, A.; Zhou, C. *ACS Nano* **2010**, *4*, 11−14.
(7) Wu, Z.; Chen, Z.; Du, X.; Logan, J. M.; Sippel, J.; Nikolou, M.; Kamaras, K.; Reynolds, J.; Tanner, D. B.; Hebard, A. F.; Rinzler, A. G. *Science* **2004**, *305*, 1273−1276.
(8) Arco, L. G.; Zhang, Y.; Schlenker, C. W.; Ryu, K.; Thompson, M. E.; Zhou, C. *ACS Nano* **2010**, *4*, 2865−2873.
(9) Lee, J. Y.; Connor, S.T.; Cui, Y.; Peumans, P. *Nano Lett.* **2008**, *8*, 689−692.
(10) De, S.; Higgins, T. M.; Lyons, P. E.; Doherty, E. M.; Nirmalraj, P. N; Blau, W. J.; Boland, J. J.; Coleman, J. N. *ACS Nano* **2009**, *3*, 1767−1774.
(11) Rathmell, A. R.; Bergin, S. M.; Hua, Y. L.; Li, Z. Y.; Wiley, B. J. *Adv. Mater.* **2010**, *22*, 3558−3563.
(12) Wu, H.; Hu, L.; Rowell, M. W.; Kong, D.; Cha, J. J.; McDonough, J. R.; Zhu, J.; Yang, Y.; McGehee, M. D.; Cui, Y. *Nano Lett.* **2010**, *10*, 4242−4248.
(13) Hu, L.; Kim, H. S.; Lee, J. Y.; Peumans, P.; Cui, Y. *ACS Nano* **2010**, *4*, 2955−2963.
(14) Gaynor, W.; Burkhard, G. F.; McGehee, M. D.; Peumans, P. *Adv. Mater.* **2011**, *23*, 2905−2910.
(15) Liu, C. H.; Yu, X. *Nanoscale Res. Lett.* **2011**, *6*, 75−82.
(16) Madaria, A. R.; Kumar, A.; Zhou, C. *Nanotechnology* **2011**, *22*, 245201−245206.
(17) Scardaci, V.; Coull, R.; Lyons, P. E.; Rickard, D.; Coleman, J. N. *Small* **2011**, *7*, 2621−2628.
(18) Hesjedal, T. *Appl. Phys. Lett.* **2011**, *98*, 133106.
(19) Kang, J.; Hwang, S.; Kim, J. H.; Kim, M. H.; Ryu, J.; Seo, S. J.; Hong, B. H.; Kim, M. K.; Choi, J. *ACS Nano* **2012**, *6*, 5360−5365.
(20) Chen, T. L.; Ghosh, D. S.; Krautz, D.; Cheylan, S.; Pruneri, V. *Appl. Phys. Lett.* **2011**, *99*, 093302.
(21) Chen, T. L.; Betancur, R.; Ghosh, D. S.; Martorell, J.; Pruneri, V. *Appl. Phys. Lett.* **2012**, *100*, 013310.
(22) Ghosh, D. S.; Chen, T. L.; Formica, N.; Huang, J.; Bruder, I.; Pruneri, V. *Sol. Energy Mat. Sol. C* **2012**, *107*, 338−343.
(23) Jeong, C.; Nair, P.; Khan, M.; Lundstrom, M.; Alam, M. A. *Nano Lett.* **2011**, *11*, 5020−5025.
(24) Kholmanov, I. N.; Magnuson, C. W.; Aliev, A. E.; Li, H.; Zhang, B.; Suk, J. W.; Zhang, L.; Peng, E.; Mousavi, S. H.; Khanikaev, A. B.; Piner, R.; Shvets, G.; Ruoff, R. S. *Nano Lett.* **2012**, *12*, 5679−5683.
(25) Gaynor, W.; Lee, J. Y.; Peumans, P. *ACS Nano* **2010**, *4*, 30−34.
(26) Ghosh, D. S.; Chen, T. L.; Mkhitaryan, V.; Formica, N.; Pruneri, V. *Appl. Phys. Lett.* **2013**, *102*, 221111.
(27) Tokuno, T.; Nogi, M.; Karakawa, M.; Jiu, J.; Nge, T. T.; Aso, Y.; Suganuma, K. *Nano Res.* **2011**, *4*, 1215−1222.
(28) Madaria, A. R.; Kumar, A.; Ishikawa, F. N.; Zhou, C. W. *Nano Res* **2010**, *3*, 564−573.
(29) Ajuria, J.; Ugarte, I.; Cambarau, W.; Etxebarria, I.; Zaera, R.; Pacios, R. *Sol. Energy Mat. Sol. C* **2012**, *102*, 148−152.
(30) Preston, C.; Xu, Y.; Han, X.; Munday, J. N.; Hu, L. *Nano Res.* **2013**, *6*, 461.
(31) Mattevi, C.; Kim, H.; Chhowalla, M. *J. Mater. Chem.* **2011**, *21*, 3324−3334.
(32) Deng, F.; Zheng, Q. S. *Appl. Phys. Lett.* **2008**, *92*, 071902.
(33) Deng, F.; Zheng, Q. S.; Wang, L. F.; Nan, C. W. *Appl. Phys. Lett.* **2007**, *90*, 021914.
(34) Huang, Y. Y.; Terentjev, E. M. *ACS Nano* **2011**, *5*, 2082−2089.
(35) Lotya, M.; Hernandez, Y.; King, P. J.; Smith, R. J.; Nicolosi, V.; Karlsson, L. S.; Blighe, F. M.; De, S.; Wang, Z.; McGovern, I. T.; Duesberg, G. S.; Coleman, J. N. *J. Am. Chem. Soc.* **2009**, *131*, 3611−3620.
(36) Chen, T. L.; Ghosh, D. S.; Formica, N.; Pruneri, V. *Nanotechnology* **2012**, *23*, 395603.
(37) Kim, K. S.; Zhao, Y.; Jang, H.; Lee, S. Y.; Kim, J. M.; Kim, K. S.; Ahn, J.; Kim, P.; Choi, J.; Hong, B. H. *Nature* **2009**, *457*, 706−710.
(38) Bae, S.; Kim, H.; Lee, Y.; Xu, X.; Park, J.; Zheng, Y.; Balakrishnan, J.; Lei, T.; Kim, H. R.; Song, Y.; Kim, K. S.; Ozyilmaz, B.; Ahn, J.; Hong, B. H.; Lijima, S. *Nat. Nanotech.* **2010**, *5*, 574−578.
(39) Ferrari, A. C.; Meyer, J. C.; Scardaci, V.; Casiraghi, C.; Lazzeri, M.; Mauri, F.; Piscanec, S.; Jiang, D.; Novoselov, K. S.; Roth, S.; Geim, A. K. *Phys. Rev. Lett.* **2006**, *97*, 187401.
(40) Ferrari, A. C. *Solid State Communications* **2007**, *143*, 47−57.
(41) Chen, R.; Das, S. R.; Jeong, C.; Khan, M. R.; Janes, D. B.; Alam, M. A. *Adv. Funct. Mater.* **2013**, *23*, 5150−5158.
(42) Lee, M.; Lee, K.; Kim, S.; Lee, H.; Park, J.; Choi, K.; Kim, H.; Kim, D.; Lee, D.; Nam, S.; Park, J. *Nano Lett.* **2013**, *13*, 2814−2821.
(43) Chen, J.; Jang, C.; Xiao, S.; Ishigami, M.; Fuhrer, M. S. *Nat. Nanotechnol.* **2008**, *3*, 206−209.